Polymer 51 (2010) 1820–1829

Contents lists available at ScienceDirect

Polymer

journal homepage: www.elsevier.com/locate/polymer

Effect of confinement on the relaxation behavior of poly(ethylene oxide)

C. Lai, R. Ayyer, A. Hiltner*, E. Baer

Department of Macromolecular Science and Engineering, Case Western Reserve University, Cleveland, OH 44106-7202, USA

ARTICLE INFO

Article history:
Received 31 December 2009
Received in revised form
4 February 2010
Accepted 7 February 2010
Available online 12 February 2010

Keywords:
Nanolayers
Relaxation behavior
Glass transition

ABSTRACT

It is widely thought that confinement of an amorphous polymer alters the chain mobility, which affects the temperature and intensity of the glass transition. The present study sought to determine whether the same effects extend to semicrystalline polymers. Confinement was achieved by forced assembly of hundreds of alternating layers of poly(ethylene oxide) (PEO) with either poly(ethylene-*co*-acrylic acid) or polystyrene. The confinement gradually reduced the intensity of the PEO β-relaxation as the layer thickness decreased from the microscale to the nanoscale. By considering the changes in crystalline morphology that accompanied layer confinement, it was possible to completely account for the reduction in relaxation intensity using standard mechanical models. The viscoelastic behavior of the amorphous phase was satisfactorily represented by a modified standard linear solid (SLS). The amorphous and crystalline contributions were combined using a combination of parallel and series coupling in accordance with the Takayanagi model. No adjustment in the viscoelastic parameters of the modified SLS was required, indicating that there was no significant change in amorphous chain dynamics even in layers as thin as 45 nm.

1. Introduction

The viscoelastic behavior of polymers in ultrathin films, at interfaces, and in physical confinement becomes of increasing technological and theoretical interest as applications move toward the micro- and nano-scales. To date, research has focused primarily on the glass transition (T_g) of amorphous polymers in thin and ultrathin (>10 nm) films [1,2]. A sizable body of work convincingly demonstrates a substantial influence of the air–polymer and substrate–polymer interfaces. The presence of a free surface, for example in free-standing thin films or on a coated non-interacting substrate, generally results in a decrease in T_g due to the enhanced segmental mobility [3,4]. The magnitude of the effect depends on the polymer, but is up to 35 °C in polystyrene (PS) [5]. The decrease in T_g can be eliminated, and even reversed to an increase in the T_g, if the polymer interacts with the substrate [6].

The dynamics of polymer chains confined within small pores has been studied primarily to address questions concerning the length scale that controls the molecular motions of the glass transition. For these studies, the required dimension of the confinement is less than 20 nm. The confinement is imposed by imbibing the polymer into a nanoporous inorganic glass [7–9], or intercalation in a layered silicate [10]. As with thin films, confinement and substrate interactions produce opposing effects. The confinement effect leads to an acceleration of the segmental dynamics (confinement effect) compared to the bulk. The molecular dynamics of the confined glass is also influenced by surface interactions (adsorption effect), which generally retard relaxation processes. Thus, there is a counterbalance between confinement and adsorption effects.

There is little information available on the viscoelastic behavior of confined semicrystalline polymers. Rigid confinement at a size scale below 20 nm appears to inhibit crystallization of polymers that would normally crystallize in the bulk [9]. However, crystallization proceeds readily when the confinement occurs at a size scale equal to or larger than the lamellar thickness, approximately 20 nm, or in supported ultrathin films with a free surface [11]. A decrease in the T_g of poly(L-lactic acid) films below a thickness of 50 nm was interpreted in terms of a disentanglement effect near a non-interacting surface [12]. Rigidly confined thin films without a free surface can be fabricated by microlayer coextrusion [13,14]. As the thickness of a confined poly(ethylene oxide) (PEO) layer decreases from the microscale to the nanoscale, the morphology systematically changes from three-dimensional spherulites to two-dimensional discoids and to 'in-plane' lamellar stacks [15]. Finally, when the confinement occurs on the 25 nm size scale of the usual lamellar thickness, the PEO layers crystallize as single lamellae with large aspect ratio that resemble large single crystals [16]. However, it is not known how the confinement affects the amorphous phase.

In the bulk, it is generally observed that crystallization has the effect of broadening, weakening and shifting the T_g to higher temperatures. The increase in T_g of 10–20 °C is due to restricted amorphous chain mobility imposed by connectivity to the rigid

* Corresponding author.
E-mail address: ahiltner@case.edu (A. Hiltner).

0032-3861/$ – see front matter © 2010 Elsevier Ltd. All rights reserved.
doi:10.1016/j.polymer.2010.02.016

crystals. Preventing the normal isotropic spherulitic organization by confining crystallization to two-dimensions may affect the dynamics of the noncrystalline chain segments. In this work, we advance some results showing the impact of confined crystallization on the glass transition and mechanical stress–strain properties of PEO. For this purpose, PEO was coextruded as microlayer and nanolayer films with up to 1025 layers of PEO alternating with poly (ethylene-*co*-acrylic acid) (EAA) or PS. The number of layers was adjusted in order to achieve individual layer thicknesses ranging from a few microns to 45 nm. With little or no crystallinity, EAA and PS were suitable substrates for assessing the effect of PEO crystallization habit on the mechanical relaxation behavior. Conventional experimental methods were used and the results were amenable to analysis with standard mechanical models.

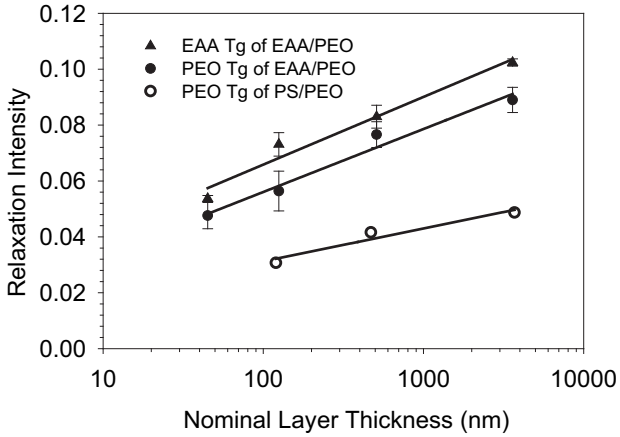

Fig. 2. Comparison of β-relaxation intensities vs. layer thickness for EAA/PEO and PS/PEO systems.

2. Materials and methods

The poly(ethylene oxide) (PEO) was Polyox WSR-N80 with a molecular weight of ~200,000 g/mol, crystallinity of about 70%, and melting point of 65 °C. The confining layers were polystyrene (PS), Styron 666, or an ethylene-*co*-acrylic acid copolymer (EAA), Primacor 1410. The PS had a glass transition temperature at 100 °C. The EAA had 9.7% acrylic acid, about 30% crystallinity with a melting temperature at 99 °C. The polymers were obtained from The Dow Chemical Company. The resins used in this study were previously found to be immiscible in melt blends [17].

Films with 33, 257, and 1025 alternating PEO and PS or EAA layer with 50/50 (vol/vol) composition were produced through the continuous coextrusion process described previously [13,14,16]. Varying the number of layers allowed for a large range of layer thicknesses. The overall film thicknesses ranged from 50 μm to130 μm, which corresponded to individual PEO layer thicknesses from 45 nm to 3700 nm. There was some variation in layer thickness [15], however any effect of layer thickness was averaged out in measurements of the bulk properties. The films were kept dry in a desiccator with molecular sieves before all testing.

The crystallinity was measured using differential scanning calorimetry (DSC). Thermograms were obtained on a Perkin Elmer (Boston, MA) Series 7 DSC at a heating/cooling rate 10 °C min^{-1}. The weight fraction PEO crystallinity was converted to volume fraction according to

$$V_c = \frac{\rho_a W_c}{[\rho_a W_c + \rho_c(1 - W_c)]} \quad (1)$$

where, V_c is the volume fraction crystallinity, W_c is the weight fraction crystallinity, ρ_c is the crystalline phase density (1.239 g/cm^3), and ρ_a is the amorphous phase density (1.124 g/cm^3) [18]. The volume crystallinity was 73% for the PEO control and 71% for all layered films.

Dynamic mechanical testing was performed on a Polymer Laboratories (Boston, MA) MkII dynamic mechanical thermal analyzer in tension. Rectangular samples with dimensions of 35 mm by 8 mm ($n = 3$) were cut from the extruded films along the extrusion direction along the same line. Thickness was measured using a digital micrometer, and width was measured with a digital caliper. The length to be tested in the DMTA was set to 13 mm for every sample. Each rectangular sample was tested at 1 Hz, strain of 11 μm, from −110 °C to 100 °C, heating at 3 °C/min. Experiments were stopped when the displacement exceeded 1500 μm.

The stress–strain behavior in uniaxial tension was measured with ASTM D1708 microtensile specimens cut from the extruded EAA/PEO films along the extrusion direction. Specimens were stretched in an MTS (Eden Prairie, MN) Alliance RT30 mechanical testing machine at a strain-rate of 5% min^{-1} at a temperature of −10 °C. Engineering stress and strain were defined conventionally. The tensile modulus was taken at 1% strain.

To change the crystalline structure of the PEO layers, the films were heated to a temperature above the melting temperature of PEO but below the softening temperature of the confining layer, and quenched. The films were sandwiched with aluminum foil and the edges sealed with super glue. They were immersed in a hot oil bath at 70–75 °C for EAA/PEO or 85–90 °C for PS/PEO for 10 min to melt the PEO layer within the rigid confinement of the PS or EAA

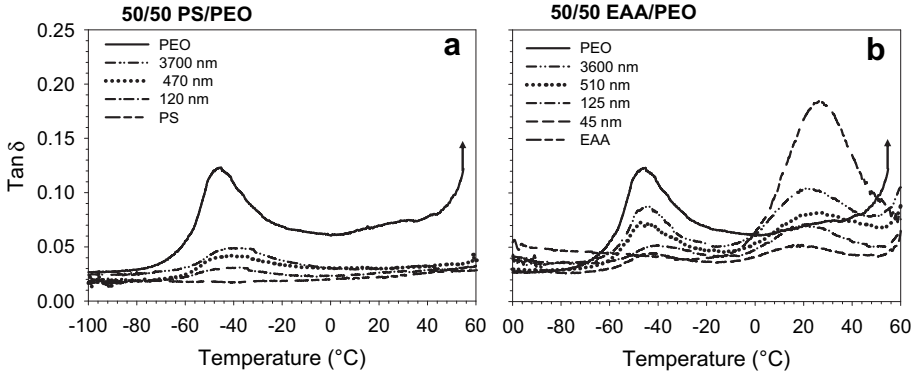

Fig. 1. Dynamic mechanical tan δ curves showing the reduction in β-relaxation intensity with decreasing layer thickness: (a) Curves for 50/50 PS/PEO and controls; and (b) curves for 50/50 EAA/PEO and controls.

layers. The PEO was recrystallized by rapidly transferring the masked samples to liquid nitrogen and holding them there for 15–20 min. The aluminum masking was removed for further characterization.

The WAXD measurements were performed using a rotating anode X-ray generator (RU 300, 12 kW, Rigaku, Woodlands, TX). The PD and ND WAXD patterns were collected with the monochromatic X-ray beam parallel to the plane of the film (PD). The collimated beam size was ~0.5 mm. The 2D patterns were collected with a Bruker AXS (Madison, WI) HI-STAR area detector. The sample-to-detector distance was 74 mm and the diffraction angle was calibrated using a CaF_2 standard.

3. Results and discussion

3.1. Dynamic mechanical behavior

The DMTA tan δ curves for PS/PEO and EAA/PEO layered films, and their controls are plotted in Fig. 1. The intense β-relaxation at −45 °C corresponded to the PEO glass transition [19]. The intensity was reduced in films with thick 3.7 micron layers due to the 50/50 composition. As the PEO layers became thinner, the intensity diminished further, even though the composition and crystallinity remained constant. The observed temperature of the relaxation remained relatively unchanged at −41 °C to −43 °C, only 3–5 °C higher than for the PEO control, and the peak width appeared unaffected. The EAA exhibited a β-relaxation peak at 25 °C that corresponded with the glass transition reported for an EAA of similar comonomer content [20]. This relaxation peak intensity also decreased as the layers became thinner. The peak gradually shifted to lower temperatures, by about 10 °C.

A linear relationship between relaxation intensity and the log of the nominal PEO layer thickness can be seen in Fig. 2 for both PS/PEO and EAA/PEO films. The intensity was taken at the peak maximum after the baseline was subtracted. Comparing the PEO in the two systems, it can be seen that the peak was about twice the intensity in EAA/PEO films as in PS/PEO films of similar PEO layer thickness. In the EAA/PEO system, the β-relaxation intensity of the EAA layers decreased in parallel with the PEO relaxation.

It is significant that changes in the relaxation peak intensities were observed in relatively thick layers. This characteristic, together with the negligible changes in peak temperature and peak width, suggested that the intensity changes were not a substrate effect. An alternative explanation needed to account for both the decrease in the PEO β-relaxation and the parallel decrease in the β-relaxation of the confining EAA layers. For this purpose, we considered the stress distribution within the PEO layers and also the stress distribution between the PEO layers and the confining layers. Previously it was established that without a change in the crystallinity, the morphology of the PEO layer changed from isotropic 3-dimensional spherulites to 2-dimensional discoids and finally to highly oriented, in-plane lamellae as the confined PEO layer thickness decreased from the microscale to the nanoscale [15]. As the PEO lamellae lengthened and became more aligned in the loading direction, it is proposed that the load was redistributed with increased load carried by the crystalline phase. Because less of the load was born by the amorphous phase, the intensity of the amorphous phase β-relaxation was reduced. Furthermore, the reinforcing effect of the long, oriented lamellae increased the modulus of the PEO layers in the loading direction of the dynamic mechanical experiment. This reduced the load on the unoriented confining layers of the parallel construction and the intensity of the EAA β-relaxation correspondingly decreased. The confining PS

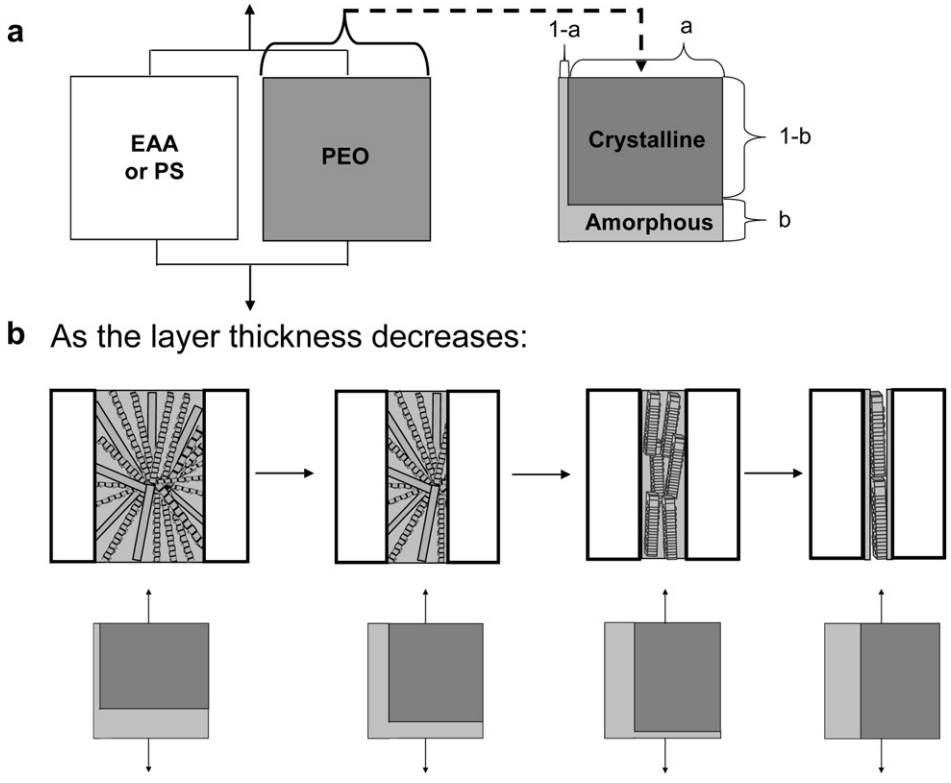

Fig. 3. The mechanical model for the PEO layers: (a) The composite parallel system with the PEO layers described by the Takayanagi model; and (b) schematics showing the effect of layer thickness on the lamellar organization and the corresponding changes in the mechanical model.

Table 1
Tensile modulus of EAA/PEO films (5%/min, −10 °C), the extracted modulus of the PEO layers, and the corresponding input values to the Takayanagi model for the PEO layers.

Sample	1% Modulus (MPa)	1% PEO Modulus (MPa)	*a*	*b*
EAA Control	670 ± 40	–	–	–
PEO Control	540 ± 20	540 ± 20	0.7223	0.0170
50/50 3600 nm	730 ± 80	790 ± 120	0.7175	0.0105
50/50 510 nm	940 ± 30	1210 ± 70	0.7140	0.0056
50/50 125 nm	1060 ± 50	1450 ± 90	0.7129	0.0041
50/50 45 nm	1240 ± 50	1820 ± 90	0.7119	0.0026

layers did not have any relaxations in the temperature range examined.

3.2. Modeling the two-phase structure of PEO

The semicrystalline PEO layers are considered as consisting of a crystalline phase dispersed in a continuous amorphous matrix. The 2-phase structure is modeled as a series combination of a discontinuous amorphous part and a crystalline part assembled in parallel with a continuous amorphous part, Fig. 3a, according to the Takayanagi configuration [21,22]. The relative contributions of the series and parallel components are adjusted to accommodate thickness-dependent morphology changes, which are assumed to occur only in the PEO layers and not in the confining layers. Subsequently, the layered film is constructed as a parallel arrangement of oriented semicrystalline PEO layers and isotropic confining layers.

The crystalline phase has dimensions a and $(1-b)$, with an area $a(1-b)$ equal to the crystalline volume fraction V_c. The total amorphous phase with volume fraction $1-V_c$ is equal to the total area of the two amorphous parts $1-a+ab$. As the layer thickness decreases, the morphology change is represented by changes in the parameters a and b of the model. This is represented schematically in Fig. 3b. The spherulitic morphology of thick PEO layers resembles that of the PEO control, represented by a thicker discontinuous amorphous phase, and a thinner continuous amorphous phase. Reducing the layer thickness aligns the PEO lamellae along the direction of the layers, increasing $1-b$, and decreasing a. In the thinnest layers, the lamellae approach a parallel configuration, with a single continuous crystalline part in parallel with a continuous amorphous part.

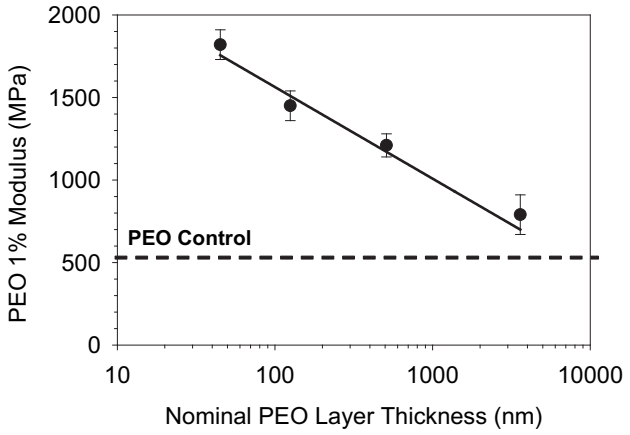

Fig. 4. The tensile modulus of PEO layers vs. nominal PEO layer thickness showing the increase in PEO modulus with decreasing layer thickness. Measurements were made on the EAA/PEO system at −10 °C and 5%/min.

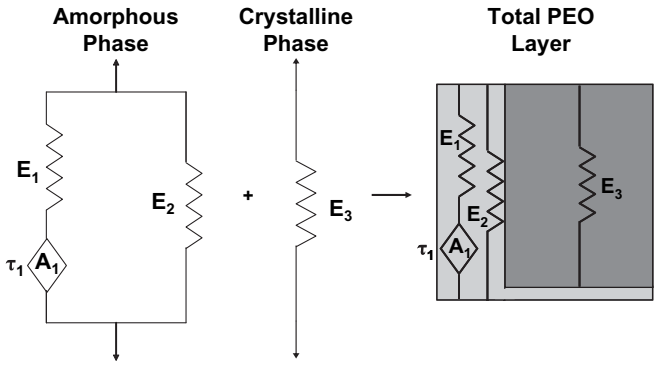

Fig. 5. Combination of a modified standard linear solid model, representing the amorphous phase, with a crystalline spring according to the Takayangi model.

The elastic modulus in the 2-phase Takayanagi model is expressed by [21,22]

$$E_{PEO} = a\left[\frac{b}{E_{am}} + \frac{(1-b)}{E_c}\right]^{-1} + (1-a)E_{am} \quad (2)$$

where E_{PEO} is the elastic modulus of the PEO layer, E_{am} is the modulus of the amorphous parts, and E_c is the modulus of the crystalline part. The area of the crystalline region V_c can be expressed in terms of a and b

$$a = \frac{V_c}{(1-b)} \quad (3)$$

Equation (2) can be simplified to a single unknown

$$E_{PEO} = \frac{V_c}{(1-b)}\left[\frac{b}{E_{am}} + \frac{(1-b)}{E_c}\right]^{-1} + \left(1 - \frac{V_c}{(1-b)}\right)E_{am} \quad (4)$$

The parameters a and b were obtained from the tensile modulus of the PEO layer. For that purpose, the composite modulus of the layered film was measured and E_{PEO} was extracted using the parallel model

$$E_{composite} = E_{PEO}V_{f,PEO} + E_{EAA}V_{f,EAA} \quad (5)$$

The modulus of the control films determined at ambient temperature followed well with literature values [23,24]. However, for this study, the tensile modulus of the EAA/PEO films was measured at −10 °C, which was intermediate between the β-relaxations of PEO and EAA where the loss was lowest. Because the modulus decreased rapidly between −10 °C and ambient temperature, the values obtained at −10 °C were substantially higher than the usual ambient temperature values. The results for EAA/PEO films and the controls at −10 °C are reported in Table 1. The changes in the modulus of layered films were attributed to the PEO layer only. The modulus of the EAA layers was assumed to remain constant based on the previous finding that layer thickness affected the orientation of the PEO layers, but not of the low crystallinity EAA layers [16]. The extracted PEO modulus increased with the PEO layer thickness logarithmically, Fig. 4. In the thinnest layers, the modulus was about 3× that of the control. As the layer thickness increased, the modulus decreased, approaching that of the control in the thickest layers, Table 1.

To determine the parameters a and b, E_{am} was assumed to be equivalent to a typical rubbery modulus of 15 MPa [24,25], and E_c was assigned a reported value of 4.6 GPa [26]. Applying equation (4), b was varied to match the measured PEO modulus, and a was then calculated using equation (3). The results are summarized in Table 1. As expected, b decreased, approaching zero, in the thinnest layers.

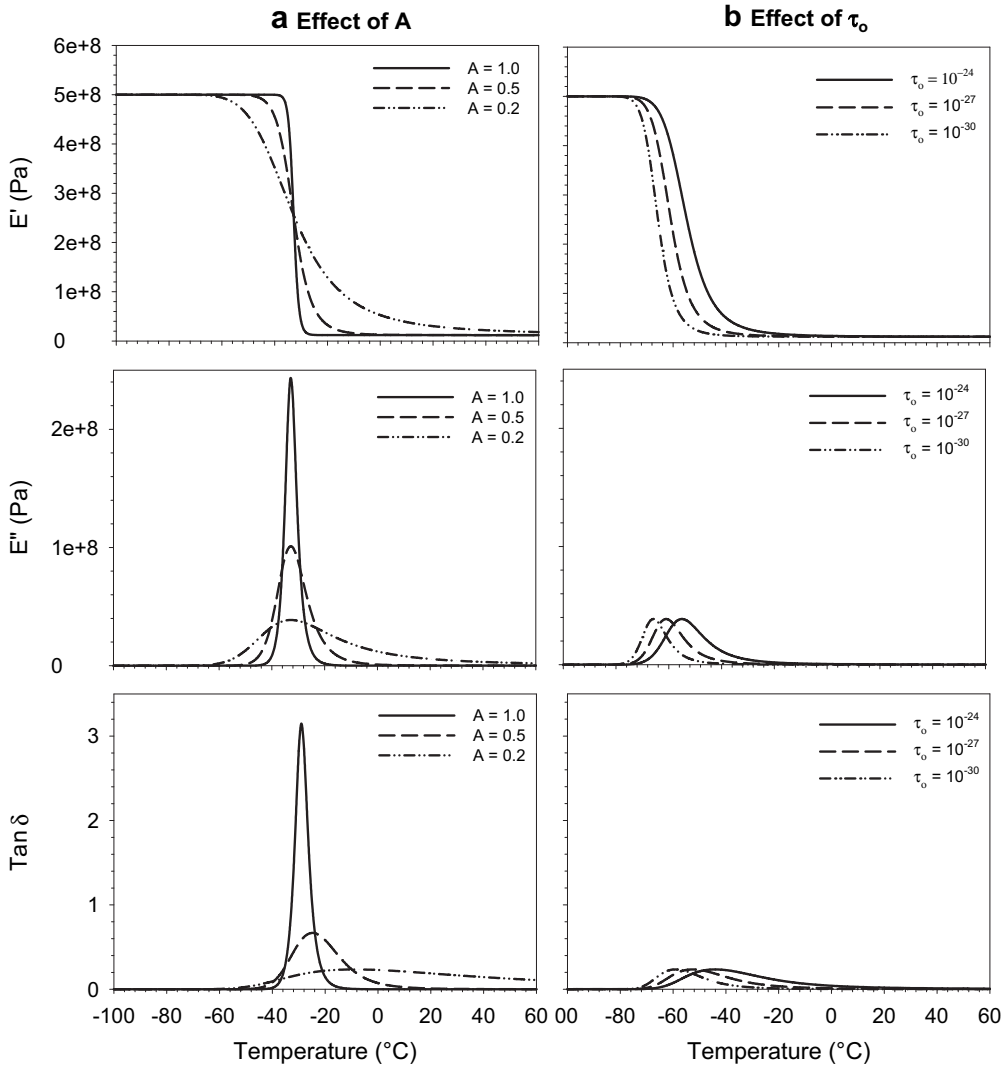

Fig. 6. Effect of input values on the SLS model response: (a) Spring-pot parameter A for $\tau_o = 1 \times 10^{-17}$ s; and (b) relaxation time pre-exponential factor τ_o for $A = 0.2$.

3.3. Dynamic response of PEO

To model the dynamic response in the β-relaxation region, the PEO was considered to consist of an elastic crystalline phase and a viscoelastic amorphous phase, Fig. 5. The temperature dependent response of the amorphous phase was elicited using a modified standard linear solid (SLS) model in which the dashpot of the classical Zener model is replaced with a spring-pot [27]. In the model, a series combination of a spring with glassy modulus E_1 and a spring-pot is combined in parallel with a spring with rubbery modulus E_2. At lower temperatures, the amorphous phase is in the glassy state and there is no response from the spring-pot due to its high viscosity. The model response is governed primarily by E_1 as $E_2 \ll E_1$. At higher temperatures, well above the β-relaxation, the spring-pot is fluid and the model response is governed by the rubbery modulus E_2. In the region of the β-relaxation, the viscosity of the spring-pot determines the model response.

The storage and loss moduli for the modified SLS model are described by [27]:

$$E'_{SLS}(T) = E_1 - \frac{(E_1 - E_2)\left[1 + (\omega\tau(T))^A \cos\left(A\frac{\pi}{2}\right)\right]}{\left[1 + (\omega\tau(T))^A \cos\left(A\frac{\pi}{2}\right)\right]^2 + \left[(\omega\tau(T))^A \sin\left(A\frac{\pi}{2}\right)\right]^2} \tag{6}$$

$$E''_{SLS}(T) = \frac{(E_1 - E_2)\left[1 + (\omega\tau(T))^A \sin\left(A\frac{\pi}{2}\right)\right]}{\left[1 + (\omega\tau(T))^A \cos\left(A\frac{\pi}{2}\right)\right]^2 + \left[(\omega\tau(T))^A \sin\left(A\frac{\pi}{2}\right)\right]^2} \tag{7}$$

where, E_1 and E_2 are the moduli of the amorphous glass and the rubber, respectively. These were varied within a range of typical values for a glass (400–1500 MPa), and a rubber (1–50 MPa) [25]. The testing frequency ω was 1 Hz. The spring-pot parameter A can take values between 0 and 1. The temperature dependent relaxation time spectrum $\tau(T)$ is expressed as

$$\tau(T) = \tau_0 \left(\exp\left(\frac{E_a}{kT}\right)\right)^Z \tag{8}$$

The Z exponent is calculated from

$$Z(T) = \frac{T\left(T^* - T_0\right)}{T^*(T - T_0)} \tag{9}$$

where T^* is the melting temperature, T_o is a temperature below the glass transition, and k is the Boltzmann's constant.

The effect of the spring-pot parameters on the relaxation characteristics of the modified SLS model was examined. Decreasing A broadened the relaxation and decreased the intensity of the loss modulus and tan δ peaks, Fig. 6a. The pre-exponential factor τ_o in the expression for $\tau(T)$ affected the transition temperature, as well as the distribution, although τ_o did not affect the distribution as strongly as the A parameter did, Fig. 6b. Decreasing E_a shifted the relaxation to lower temperatures and slightly narrowed the relaxation, although the effect was small compared to that of the other two parameters. Varying T_o shifted the peak position in the dynamic response.

The modified SLS model for the PEO amorphous phase was combined with the crystalline phase of elastic modulus E_3 as shown in Fig. 5. Expressions for the storage and loss moduli of the Takayanagi model were taken from the literature [28]

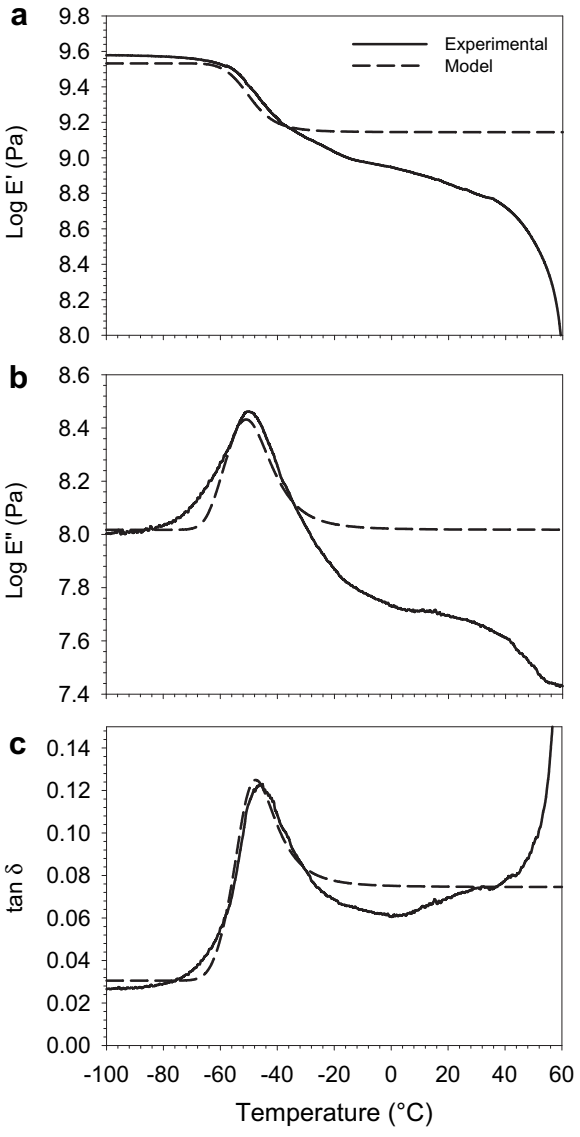

Fig. 7. Comparison of PEO model response with experimental results for the PEO control: (a) Storage modulus; (b) loss modulus; and (c) tan δ.

$$E'_{PEO} = (1-a)E'_{am} + \frac{a\left[E'_{am}E'_c - E''_{am}E''_c\right]\left[(1-b)E'_{am} + bE'_c\right]}{\left[(1-b)E'_{am} + bE'_c\right]^2 + \left[(1-b)E''_{am} + bE''_c\right]^2} + \frac{a\left[E'_{am}E''_c + E''_{am}E'_c\right]\left[(1-b)E''_{am} + bE''_c\right]}{\left[(1-b)E'_{am} + bE'_c\right]^2 + \left[(1-b)E''_{am} + bE''_c\right]^2} \tag{10}$$

$$E''_{PEO} = (1-a)E''_{am} + \frac{a\left[E'_{am}E''_c + E''_{am}E'_c\right]\left[(1-b)E'_{am} + bE'_c\right]}{\left[(1-b)E'_{am} + bE'_c\right]^2 + \left[(1-b)E''_{am} + bE''_c\right]^2} - \frac{a\left[E'_{am}E'_c - E''_{am}E''_c\right]\left[(1-b)E''_{am} + bE''_c\right]}{\left[(1-b)E'_{am} + bE'_c\right]^2 + \left[(1-b)E''_{am} + bE''_c\right]^2} \tag{11}$$

Substitution of equations (6) and (7) gave the temperature dependent response as

$$E'_{PEO}(T) = (1-a)E'_{SLS}(T) + \frac{a\left[E'_{SLS}(T)E_3\right]\left[(1-b)E'_{SLS}(T) + bE_3\right]}{\left[(1-b))E'_{SLS}(T) + bE_3\right]^2 + \left[(1-b)E''_{SLS}(T)\right]^2} + \frac{a\left[E''_{SLS}(T)E_3\right]\left[(1-b)E''_{SLS}(T)\right]}{\left[(1-b)E'_{SLS}(T) + bE_3\right]^2 + \left[(1-b)E''_{SLS}(T)\right]^2} \tag{12}$$

$$E''_{PEO}(T) = (1-a)E''_{SLS}(T) + \frac{a\left[E''_{SLS}(T)E_3\right]\left[(1-b)E'_{SLS}(T) + bE_3\right]}{\left[(1-b)E'_{SLS}(T) + bE_3\right]^2 + \left[(1-b)E''_{SLS}(T)\right]^2} - \frac{a\left[E'_{SLS}(T)E_3\right]\left[(1-b)E''_{SLS}(T)\right]}{\left[(1-b)E'_{SLS}(T) + bE_3\right]^2 + \left[(1-b)E''_{SLS}(T)\right]^2} \tag{13}$$

The crystalline modulus E_3 was assigned a value of 4.6 GPa, taken from the literature [26]. Values for a and b were taken from Table 1. The melting temperature T^* was 338–340 K (65–67 °C) for PEO. The other input values of A, τ_o, E_a, and T_o for the modified SLS model were adjusted through an iterative process to optimize the fit of the combined model response to the experimental PEO control in relaxation distribution, height, and position. Adjusting A and τ_o allowed for good control of the peak height through A, while maintaining the distribution through τ_o. The activation energy E_a for the PEO β-relaxation was varied within a set of literature values, 25–147 kJ/mol [29,30]. Lower E_a values shifted the relaxation to lower temperatures and narrowed it slightly. In conjunction with A and τ_o, E_a was used to fit the position, shape, and height of the model response, although the effect of E_a was small compared to that of the other two parameters. The temperature T_o was varied to shift the peak position. After the best fit was obtained, a baseline of 1×10^8 Pa was added to the loss modulus to match the experimental baseline. Finally, tan δ was extracted from the fits of E' and E''.

The fits of the model to the experimental data for storage modulus, loss modulus, and tan δ of the PEO control are shown in

Table 2
Optimized model parameters for PEO.

Parameter	PEO
A1	0.226
τ_o (s)	10^{-30}
E_a (J/molecule)	9.14×10^{-20}
E_1 (Pa)	1.0×10^9
E_2 (Pa)	5.5×10^7
E_3 (Pa)	4.60×10^9
$T^* = T_m$ (°C)	66
T_o (°C)	−107
ω (Hz)	1

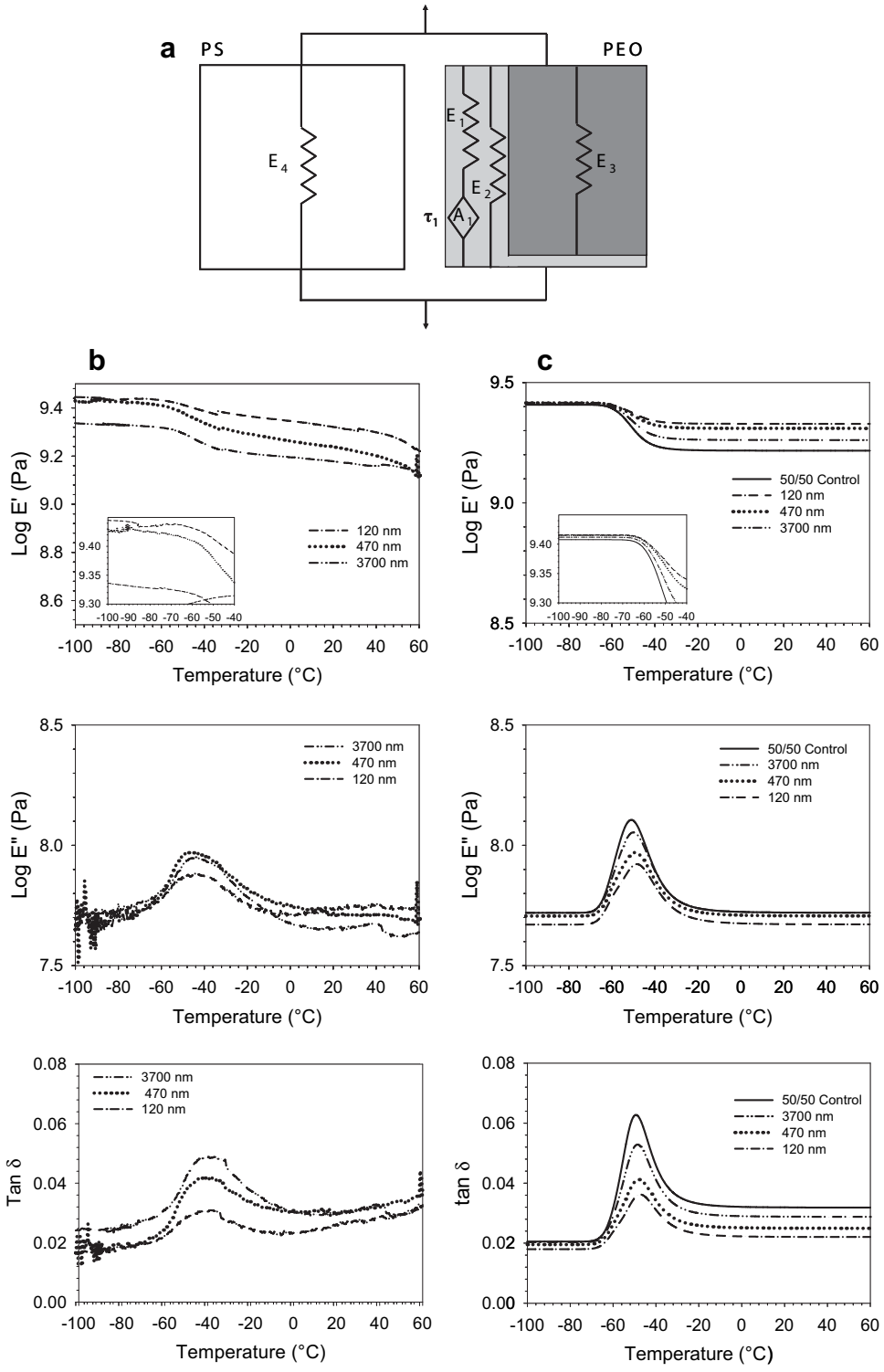

Fig. 8. Comparison of experiment and model for PS/PEO; (a) Schematic of the PS/PEO composite system; (b) experimental results; and (c) model response.

Fig. 7a–c. The storage modulus agreed very well with the experimental data in the transition region. The loss modulus, after shifting the baseline, almost completely emulated the experimental data through the transition. The tan δ response was in very good agreement with the experimental curve, with very similar peak temperature, shape and height. The resulting optimized input values for the PEO control are given in Table 2. These input values were utilized to describe the PEO layer in subsequent calculations of the layered systems.

3.4. Dynamic response of the layered systems

The PS/PEO system was modeled by combining the two-phase PEO model in parallel with a spring to represent the PS layers, Fig. 8a. The PS elastic spring modulus E_4 was taken as the measured storage modulus of the glassy PS control, 1.85×10^9 Pa. A baseline of $4–6 \times 10^7$ Pa was added to the calculated loss modulus. The shift was about half that used for fitting the PEO control. The layered model response closely mimicked the experimental results, Fig. 8b and c. Most

importantly, the model reproduced the decrease in the PEO β-relaxation intensity with decreasing layer thickness. The response calculated for a PEO layer with the Takayanagi parameters (a and b) of the control is included as the solid line in Fig. 8c. It shows that a noticeable confinement effect is predicted even in the thickest PEO layers. The model also reproduced the experimental storage and loss moduli fairly well. Some inconsistencies may have resulted from the sensitivity of these measurements to the specimen dimensions.

The confining EAA layers of the EAA/PEO films also displayed a β-relaxation at about 27 °C that exhibited a parallel decrease in intensity with the PEO layers. The viscoelastic response of the EAA layers was represented with a modified SLS element. In this case, the low level of crystallinity was omitted from the model. The input values were chosen to match the storage and loss moduli in the β-relaxation region, Table 3. The optimized input values gave good agreement with the experimental storage and loss moduli, as shown in Fig. 9a–b. The resulting tan δ response fit the β-relaxation peak in shape and position, although the intensity was somewhat higher, Fig. 9c.

The modified SLS model for EAA was combined in parallel with the PEO model as shown schematically in Fig. 10a. The PEO loss modulus response was shifted by 4–6 $\times$ 10^7 Pa to match the experimental baseline. The model successfully reproduced the trends observed in the experimental data, as seen in Fig. 10b and c. In particular, the model reproduced the decreases in both β-relaxations with decreasing layer thickness. There was good correlation in the peak intensities for the PEO layers. The experimental EAA intensities were higher than predicted, probably due to the rapid increase of damping as the temperature approached the melting region of PEO.

3.5. Effect of lamellar orientation

The model was further tested by melting the highly oriented, in-plane PEO lamellae and quenching the film to obtain a different PEO crystallization habit. The wide-angle X-ray diffraction pattern in the extrusion direction confirmed a change in the lamellar orientation in the EAA/PEO films with 125 nm layer thickness, Fig. 11. The PEO (120) reflections appeared as equatorial arcs in the pattern of the extruded film, indicating that the PEO lamellae were oriented parallel to the layer plane [15]. In the quenched film, appearance of the PEO (120) reflections in a four-point pattern indicated that PEO crystallized as short lamella that were preferentially oriented perpendicular to the layer plane [31]. In this orientation, the short lamellae would have been highly interconnected by amorphous tie chains and the reinforcing effect of the crystals would have been similar that in the isotropic spherulite.

Fig. 12 compares the 1% tensile modulus of the PEO layers with in-plane and on-edge PEO crystal orientation. In contrast to the extruded films, the modulus of the quenched PEO layers did not change with the layer thickness. The quenched films exhibited slightly higher crystallinity than the extruded films, about 78% compared to 71% for the extruded films, which accounted for the slightly higher modulus of the thickest PEO layers. Because the quenched PEO layers were similar in crystallinity and modulus regardless of the thickness, it followed that the Takayanagi parameters (a and b) were constant, independent of layer thickness. Then, according to the stress distribution model demonstrated for the extruded films, the dynamic mechanical behavior of the quenched films should not depend on layer thickness.

The storage modulus, loss modulus, and tan δ of the quenched PS/PEO and EAA/PEO films are shown in Fig. 13a and b. It can be seen that the quenched films exhibited almost identical storage modulus, loss modulus, and tan δ regardless of the layer thickness. Eliminating the layer thickness effect by removing the in-plane orientation of the PEO lamellae supported the hypothesis that the large reduction of the β-relaxation intensity seen in the extruded films was due to the gradual change in crystallization habit as the layer thickness decreased from spherulites with nearly isotropic lamellar orientation to large, highly oriented in-plane lamellae.

Table 3
Optimized model parameters for EAA.

Parameter	EAA
A_2	0.255
τ_o (s)	10^{-28}
E_a (J/molecule)	2.01×10^{-19}
E_5 (Pa)	4.50×10^8
E_6 (Pa)	4.50×10^7
$T^* = Tm$ (°C)	99
T_o (°C)	−112
ω (Hz)	1

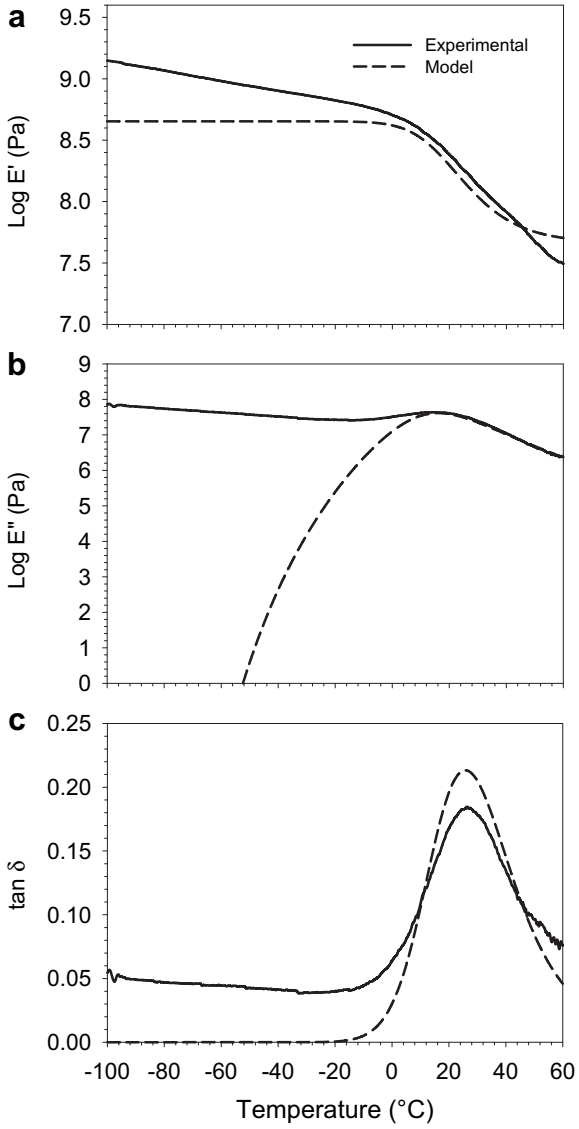

Fig. 9. Comparison of EAA model response with experimental results for the EAA control: (a) Storage modulus; (b) loss modulus; and (c) tan δ.

4. Conclusions

It is widely suggested that confinement of an amorphous polymer in thin spaces reduces the chain mobility, which is manifest as

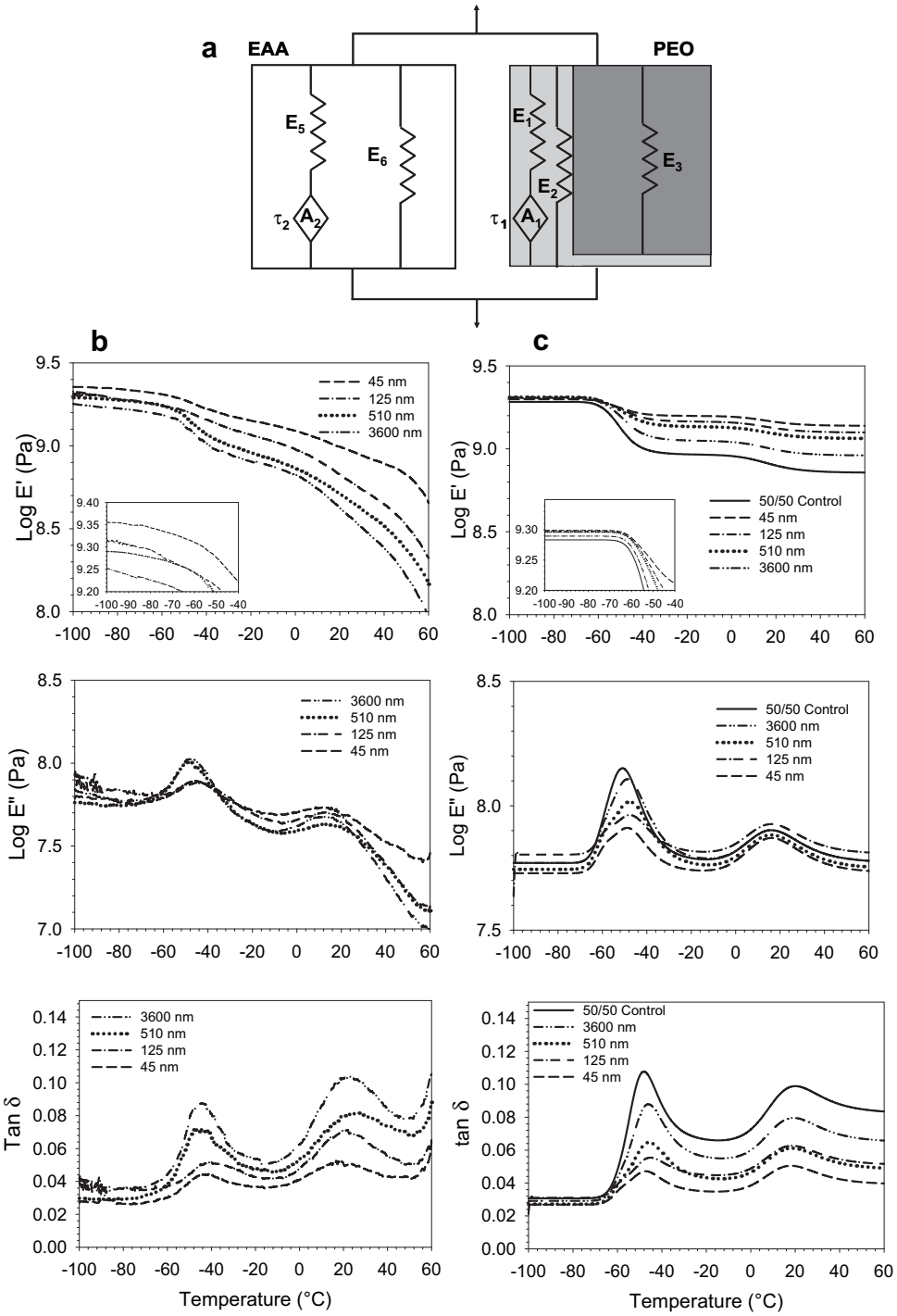

Fig. 10. Comparison of experiment and model for EAA/PEO; (a) Schematic of the EAA/PEO composite system; (b) experimental results; and (c) model response.

a reduction in the β-relaxation intensity. The presence of a crystalline phase imposes additional constrains on the amorphous chains due to attachment to the crystals. The present study sought to determine whether concepts developed for confined amorphous polymers extend to semicrystalline polymers. For this purpose, long range, almost defect free confinement was achieved by forced assembly of hundreds of alternating layers of PEO with a minimally interacting confining polymer. The confinement gradually reduces the intensity of the PEO β-relaxation as the layer thickness decreases from the microscale to the nanoscale. However, the effect is observed in relatively thick layers where any influence of the substrate should be negligible. By considering the previously reported changes in crystalline morphology that accompany layer confinement, it is possible to completely account for the reduction in relaxation intensity using standard mechanical models. The viscoelastic behavior of the amorphous phase is satisfactorily represented by a modified SLS model. The amorphous and crystalline contributions are combined using a combination of parallel and series coupling in accordance with the Takayanagi model. No adjustment in the viscoelastic parameters of the modified SLS model is required, indicating that there is no change in amorphous phase mobility even in layers as thin as 45 nm. The effect

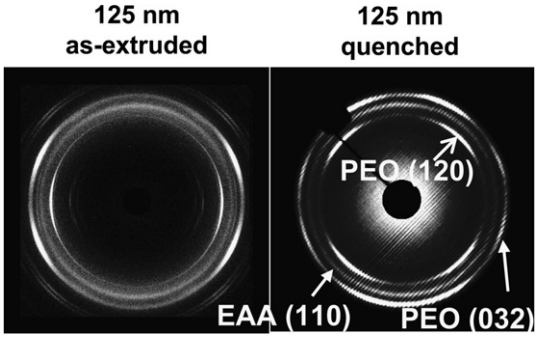

Fig. 11. 2D WAXS patterns of EAA/PEO films with 125 nm layers showing a change from in-plane lamellar orientation in the as-extruded film to on-edge lamellar orientation in the quenched film.

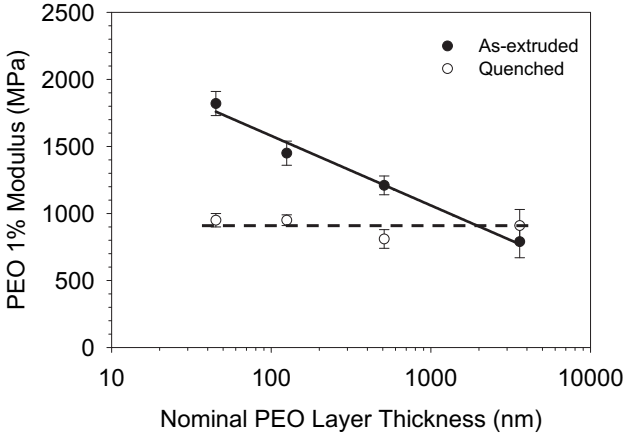

Fig. 12. The tensile modulus of PEO layers vs. nominal PEO layer thickness comparing the as-extruded and quenched EAA/PEO films. Measurements were made at −10 °C and 5%/min.

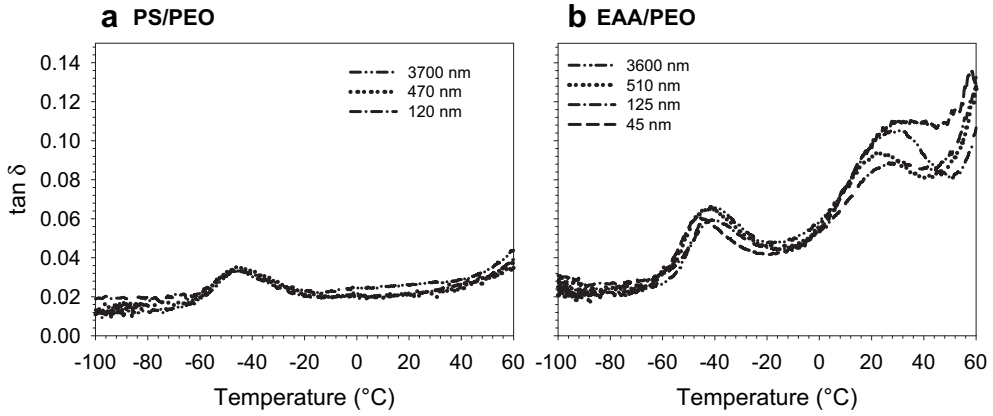

Fig. 13. Tan δ curves for quenched films: (a) PS/PEO; and (b) EAA/PEO.

of the crystalline morphology is accommodated through the independently determined parameters of the Takayanagi model, which dictate an increasing contribution of parallel coupling as the layer thickness decreases. It appears that in semicrystalline polymers the constraints imposed by attachment to crystals influence the amorphous chain mobility to a greater extent than does physical confinement. However, the situation may be different if the polymer is rigidly confined, i.e. without a free surface, at a size scale below the lamellar thickness of about 20 nm.

Acknowledgements

This research was supported by the NSF Center for Layered Polymeric Systems (grant DMR-0423914).

References

[1] Alcoutlabi M, McKenna GB. J Phys Condens Matter 2005;17:R461.
[2] Alba-Simionesco C, Coasne B, Dosseh G, Dudziak G, Gubbins KE, Radhakrishnan R, et al. J Phys Condens Matter 2006;18:R15.
[3] Fakhraai Z, Forrest JA. Science 2008;319:600.
[4] Koh YP, McKenna GB, Simon SL. J Polym Sci Part B Polym Phys 2006;44:3518.
[5] Elison CJ, Mundra MK, Torkelson JM. Macromolecules 2005;38:1767.
[6] Roth CB, Torkelson JM. Macromolecules 2007;40:3328.
[7] Schönhals A, Goering H, Brzezinka KW, Schick Ch. J Phys Condens Matter 2003;15:S1139.
[8] Schönhals A, Goering H, Schick Ch, Frick B, Zorn R. Colloid Polym Sci 2004;282:882.
[9] Travinskaya T, Shilov V, Kovernik G, Klepko V, Lipatov YuS. Compos Interfac 1998;6:297.
[10] Vaia RA, Sauer BB, Tse OK, Giannelis P. J Polym Sci Part B Polym Phys 1997;35:59.
[11] Taguchi K, Toda A, Miyamoto Y. J Macromol Sci Phys 2006;45:1141.
[12] Narladkar A, Balnois E, Vignaud G, Grohens Y. Macromol Symp 2008;273:146.
[13] Liu RYF, Jin Y, Hiltner A, Baer E. Macromol Rapid Commun 2003;24:943.
[14] Liu RYF, Bernal-Lara TE, Hiltner A, Baer E. Macromolecules 2005;38:4819.
[15] Wang H, Keum JK, Hiltner A, Baer E. Macromolecules 2009;42:7055.
[16] Wang H, Keum J, Hiltner A, Baer E, Freeman B, Rozanski A, et al. Science 2009;323:757.
[17] Pethe VV, Wang HP, Hiltner A, Baer E, Freeman B. J Appl Polym Sci 2008;110:1411.
[18] Huang P. Macromolecules 2007;40(3):526–34.
[19] Peyser P. Glass transition temperatures of polymers. In: Brandrup J, Immergut EH, editors. Polymer handbook. 3rd ed. United States of America: Wiley-Interscience; 1989.
[20] Robeson LM, Kuphal JA, Vratsanos MS. J Appl Polym Sci 1996;61:1561.
[21] Okamoto T, Takayanagi M. J Polym Sci Part C Polym Symp 1968;23:597.
[22] Takayanagi M, Imada K, Kajiyama T. J Polym Sci Part C Polym Symp 1966;15:263.
[23] www.dow.com.
[24] www.matweb.com.
[25] Gilbert DG, Ashby MF, Beaumont PWR. J Mater Sci 1986;21:3194.
[26] Kim BS, Porter RS. Macromolecules 1985;18:1214.
[27] Reyes-Melo E, Martínez-Vega J, Guerrero-Salazar C, Ortiz-Méndez U. J Appl Polym Sci 2004;94:657.
[28] Kawamoto N, Mori H, Yui N, Nitta K, Terano M. Angew Makromol Chem 1996;243:87.
[29] Mark JE. Physical properties of polymers handbook. 2nd ed. New York, NY: Springer; 2007.
[30] Törmälä P, Weber G, Lindberg JJ. Rheol Acta 1978;17:20l.
[31] Wang H, Keum JK, Hiltner A, Baer E. Macromol Rapid Comm 2010;31:356.